Solution-based direct readout surface enhanced Raman spectroscopic (SERS) detection of ultra-low levels of thiram with dogbone shaped gold nanoparticles

Benjamin Saute and Radha Narayanan*

Received 1st August 2010, Accepted 4th November 2010
DOI: 10.1039/c0an00594k

We report the use of two different sizes of dogbone shaped gold nanoparticles as colloidal substrates for surface enhanced Raman spectroscopy (SERS) based detection of ultra-low levels of thiram, a dithiocarbamate fungicide. We demonstrate the ability to use a solution based, direct readout SERS method as a quantitative tool for the detection of ultra-low levels of thiram. The two different sizes of dogbone shaped gold nanoparticles are synthesized by using the seed-mediated growth method and characterized by using UV-visible spectroscopy and transmission electron microscopy (TEM). The smaller dogbone shaped nanoparticles have an average size of 43 ± 13 nm. The larger dogbone shaped gold nanoparticles have an average size of 65 ± 15 nm. The nanoparticle concentration is 1.25×10^{11} nanoparticles per mL for the smaller dogbone shaped gold nanoparticles and is 1.13×10^{11} nanoparticles per mL for the larger dogbone shaped gold nanoparticles. Different concentrations of thiram are allowed to bind to the two different sizes of dogbone shaped gold nanoparticles and the SERS spectra are obtained. From the calibration curve, the limit of detection for thiram is 43.9 ± 6.2 nM when the smaller dogbone shaped gold nanoparticles are used as colloidal SERS substrates In the case of the larger dogbone shaped gold nanoparticles, the limit of detection for thiram is 11.8 ± 3.2 nM. The lower limit of detection obtained by using the larger dogbone shaped gold nanoparticles as colloidal substrates is due to the lightning rod effect, higher contributions from the electromagnetic enhancement effect, and larger number of surface sites for thiram to bind.

Introduction

Surface-enhanced Raman scattering (SERS) was discovered in 1977 by Van Duyne[1] and by Creighton.[2] SERS is a phenomenon in which there are greatly enhanced Raman signals when Raman scattering molecules are placed very near or attached onto metal substrates or metal nanoparticles. While of long standing fundamental importance,[3–6] its potential as a quantitative analytical tool has only recently begun to take place.[7–10] Some types of quantitative applications of SERS are biological sensing,[5,11–23] environmental monitoring,[16,24] trace analysis,[24] and explosive and contaminant detection.[5,24–26] The ability to use SERS as a quantitative analytical tool reflects advances in the ability to reproducibly synthesize and manipulate the size and shape of gold and silver nanoparticles.

The EPA have set maximum concentration limit (MCL) of <1 ng mL^{-1} for pollutants present in water. As a result, it is necessary to be able to detect ultra-low levels of pesticides, insecticides, fungicides, and other environmental pollutants. SERS has been used for the detection of different types of environmental pollutants.[27–30] SERS has also been used for the detection of polychlorinated biphenyls (PCBs).[27–29] Different types of pesticides[27–34] have also been detected by using SERS. In addition, SERS has been used for the detection of fungicides.[35–38] It is worth noting that in many of these studies, SERS is used qualitatively for identification of the different pollutants, PCBs, pesticides and fungicides as well as structural studies on the binding process. In our paper, we use SERS as a quantitative analytical tool for detecting ultra-low levels of thiram, which is a dithiocarbamate fungicide.

SERS has traditionally been conducted with gold and silver substrates as well as colloidal gold and silver nanoparticles. It has been recently shown that using cubic, block, and dogbone shaped gold nanoparticles result in ~100 times higher SERS enhancements of 4-mercaptobenzoic acid compared to spherical gold nanoparticles.[39] This SERS enhancement has been attributed to the lightning rod effect in which there is greater amount of localized electromagnetic fields at the corners and edges of the nanoparticles.[39]

We show that we can use two different sizes of dogbone shaped gold nanoparticles as colloidal SERS substrates for quantitative detection of ultralow levels of thiram, which is a dithiocarbamate fungicide. In this paper we demonstrate the ability to use a solution based, direct readout SERS method as a quantitative tool for the detection of ultra-low levels of thiram. In our method, we use two different sizes of dogbone shaped gold nanoparticles as colloidal SERS substrates for a solution based direct readout SERS based detection of ultra-low levels of thiram. Thiram has a disulfide bond which spontaneously breaks upon exposure to the gold nanoparticles and binds to the nanoparticles through the Au–S bond, which is the gold thiolate bond. It was observed that there is a lower limit of detection when the larger dogbone shaped gold nanoparticles are used as colloidal SERS substrates. Different sources that give rise to higher enhancements will also be discussed in the paper.

Department of Chemistry, University of Rhode Island, 51 Lower College Road, Kingston, RI, 02881, USA. E-mail: rnarayanan@chm.uri.edu; Fax: +1 401-874-5072; Tel: +1 401-874-2298

Experimental

Synthesis of two different sizes of dogbone shaped gold nanoparticles

The smaller dogbone shaped gold nanoparticles were synthesized by a slightly modified seed mediated growth method reported previously.[40–42] This synthesis consists of two distinct steps: preparation of the nanoparticle seeds and preparation of the nanoparticle growth solution. To prepare the seeds, 250 μL of 0.01 M $HAuCl_4$ is added to a solution containing 4.75 mL deionized water and 5 mL of 0.2 M CTAB. Next, 600 μL of ice-cold 0.01 M $NaBH_4$ is added to the solution, acting as a rapid reducing agent. The seed solution is allowed to age for approximately one hour. After the seed is aged, the growth solution is prepared. The growth solution consists of 95 mL of 0.1 M CTAB, 800 μL of 0.01 M $AgNO_3$, 5 mL of 0.01 M $HAuCl_4$, 550 μL of 0.1 M ascorbic acid, and 120 μL of the previously prepared seed solution. After the growth solution is prepared, the jar is left undisturbed overnight to allow the nucleation and growth process to occur. The resulting nanoparticle solution appears navy blue. In the case of the synthesis of larger dogbone shaped nanoparticles, the same type of seed mediated growth method was used and 0.25 M ascorbic acid is used in the growth solution instead of 0.1 M ascorbic acid.

UV-visible spectroscopic characterization

The two different sizes of dogbone shaped gold nanoparticles were characterized by using UV-visible spectroscopy to determine the surface plasmon band λ_{max} of the nanoparticles. The two different sizes of dogbone shaped nanoparticles were filtered by using a 0.22 micron PVDF syringe filter. Two mL of the dogbone shaped gold nanoparticles were placed into a quartz cuvette and placed in the sample holder of the Agilent 8453 diode array UV-visible spectrophotometer. The smaller dogbone shaped nanoparticles have a surface plasmon band λ_{max} of 671 nm and the larger dogbone shaped nanoparticles have a surface plasmon band λ_{max} of 758 nm.

Transmission electron microscopic characterization

TEM characterization allows for determination of the size and shape distributions of our gold nanoparticles. The different sizes of dogbone shaped gold nanoparticles are filtered in the same way as the UV-vis sample preparation. The nanoparticles are then centrifuged twice at 12 000 rpm for 10 minutes each time. This removes excess CTAB that is present in solution. One drop of the filtered and centrifuged nanoparticles is spotted on the TEM grid.

Size distribution analysis

The UTHSCSA ImageTool for Windows—Version 3 image analysis software was used to determine the size distributions of the two different sizes of dogbone shaped gold nanoparticles. The Distance tool in the Analysis pull-down menu is used to measure the number of pixels in the scale bar of the TEM image. Based on the number of pixels for the fixed size associated with the scale bar and measuring the number of pixels for ~200 nanoparticles in several TEM images, the size of the dogbone shaped gold nanoparticles can be calculated by dividing the number of pixels for the nanoparticles by the number of pixels of the scale bar and multiplying by the fixed size associated with the scale bar of the TEM image. We then plotted the histogram of % dogbone shaped gold nanoparticles *vs.* nanoparticle size and obtained a Gaussian fit to the histogram. From the Gaussian fit, we can determine the average size and standard deviation of the dogbone shaped gold nanoparticles.

Surface enhanced Raman spectroscopy (SERS)

The SERS spectra of thiram were obtained by using a Raman Systems R-3000QE Raman spectrometer. The laser excitation wavelength is 785 nm. One mL of the dogbone shaped gold nanoparticles with thiram bound to it is placed in a cuvette. The cuvette is placed in the self-contained dark chamber. The L cap is used since these are solution samples that are being analyzed. A 30 second integration time is used for acquisition of the SERS spectra. The SERS spectra are acquired in the range from 200 to 1800 cm^{-1}.

Results and discussion

There are a few papers in the literature which report the SERS spectra for thiram and discuss the binding modes to silver colloids and gold films.[43–45] In addition, there has been a paper in which the authors have made assignments of the SERS bands associated with thiram when it is bound to silver colloids.[35] We have developed a solution-based direct readout SERS method for quantitative detection of ultralow levels of thiram, which is a dithiocarbamate fungicide. Two different sizes of dogbone shaped gold nanoparticles have been used as colloidal SERS substrates for the detection of thiram.

Synthesis of the two different sizes of dogbone shaped gold nanoparticles

We have synthesized two different sizes of dogbone shaped gold nanoparticles by using the seed-mediated growth method described previously.[40–42] Fig. 1 shows a representative TEM image of the smaller dogbone shaped gold nanoparticles as well as the size distribution histogram with the average size of the particles. The size distributions were determined by using the ImageTool software. The smaller dogbone shaped gold nanoparticles have an average size of 43 ± 13 nm. The concentration

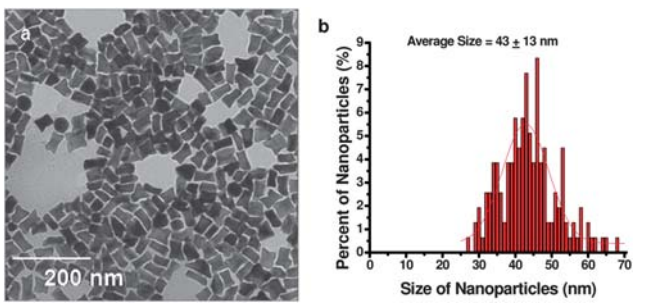

Fig. 1 TEM image of the smaller dogbone shaped gold nanoparticles (a) and size distribution histogram of the nanoparticles (b).

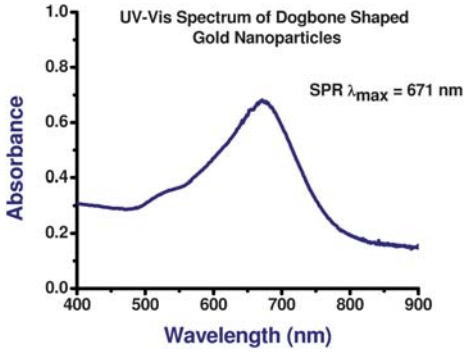

Fig. 2 UV-visible spectrum showing the surface plasmon band λ_{max} of the smaller dogbone shaped gold nanoparticles.

of the smaller dogbone shaped nanoparticles is calculated to be 1.25×10^{11} nanoparticles per mL. We have also characterized the smaller dogbone shaped gold nanoparticles by using UV-visible spectroscopy to characterize the surface plasmon band λ_{max}. It can be seen in Fig. 2 that the smaller dogbone shaped gold nanoparticles have a λ_{max} of 671 nm.

TEM images and size distribution plots were also obtained for the larger dogbone shaped gold nanoparticles. Fig. 3 shows a representative TEM image of the larger dogbone shaped gold nanoparticles as well as the size histogram with the average size of the nanoparticles. The larger dogbone shaped gold nanoparticles have an average size of 65 ± 15 nm. The concentration of the larger dogbone shaped gold nanoparticles is calculated to be 1.13×10^{11} nanoparticles per mL. We have also used UV-visible spectroscopy to obtain the surface plasmon band λ_{max}. It can be seen in Fig. 4 that the larger dogbone shaped gold nanoparticles have a surface plasmon band λ_{max} of 758 nm.

The dogbone shaped gold nanoparticles are much more attractive as colloidal SERS substrates compared to the spherical gold nanoparticles since the dogbone shaped gold nanoparticles have surface plasmon bands (671 nm and 758 nm) that are in greater resonance to the laser excitation wavelength,. The spherical gold nanoparticles have surface plasmon band in the range between 520 and 560 nm, which are not in good resonance to the laser excitation wavelength. The larger dogbone shaped gold nanoparticles have a surface plasmon band λ_{max} which is in greater resonance to the laser excitation wavelength than that of the smaller dogbone shaped gold nanoparticles. As a result, we

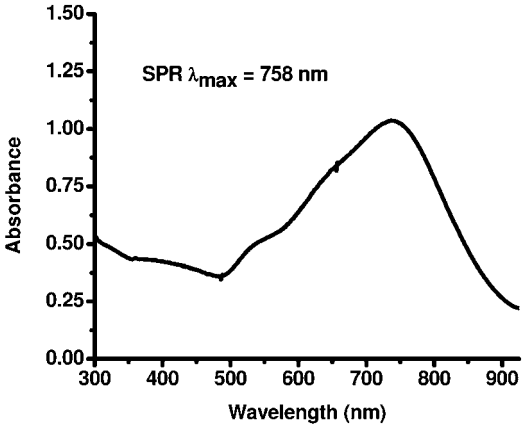

Fig. 4 UV-visible spectrum showing the surface plasmon band λ_{max} of the larger dogbone shaped gold nanoparticles.

would expect to obtain higher SERS signals using the larger dogbone shaped gold nanoparticles compared to the smaller dogbone shaped gold nanoparticles. This is discussed in more detail later on in the paper.

SERS bands of thiram

There has been a previous study where the SERS spectrum of thiram has been obtained in which the assignments of the different bands has been determined.[35] Table 1 shows the SERS peaks that we observe when the thiram is bound to the dogbone

Table 1 Table of the SERS bands associated with thiram[a]

SERS band	Assignment[35]
339 (vw)	δ (S═CS), δ (CSS)
486 (vw)	δ (CH_3NC), ν (C═S)
556 (m)	ν (SS)
755 (vw)	—
928 (m)	ν (CH_3N), ν (C═S)
1139 (m)	ρ (CH_3), ν (CN)
1379 (vs)	δ s(CH_3), ν (CN)
1444 (m)	δ as(CH_3)
1508 (m)	ρ (CH_3), ν (CN)

[a] s = strong, w = weak, m = medium, sh = shoulder, v = very, ν = stretching, δ = deformation, ρ = rocking.

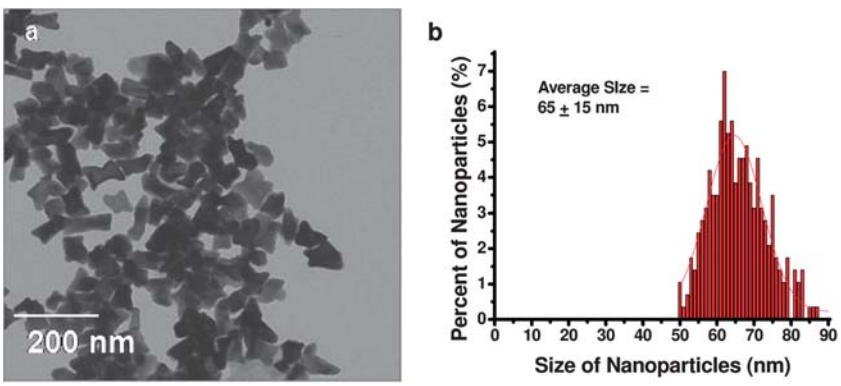

Fig. 3 TEM image of the larger dogbone shaped gold nanoparticles (a) and size distribution histogram of the nanoparticles (b).

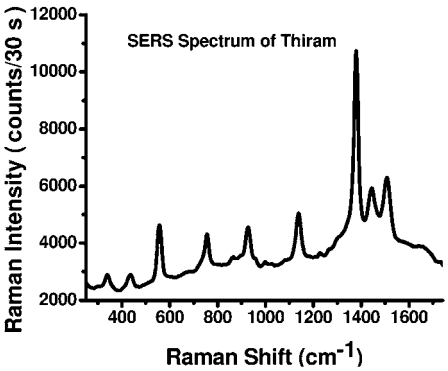

Fig. 5 Example of a SERS spectrum of thiram bound to dogbone shaped gold nanoparticles.

shaped gold nanoparticles and Fig. 5 shows an example of the SERS bands observed when thiram binds to the nanoparticles. There are many peaks in the SERS spectrum of thiram. The strongest peak is at 1379 cm^{-1} which is the CN stretching mode and symmetric CH_3 deformation mode. Since this is the strongest peak in the SERS spectra, this is the band we use for monitoring the SERS intensity as a function of the thiram concentration. The asymmetric CH_3 deformation mode occurs at 1444 cm^{-1}. The CN stretching mode also occurs at 1508 cm^{-1} as well as the rocking CH_3 mode. The CN stretching mode and rocking CH_3 mode also occurs at 1139 cm^{-1}. The stretching CH_3N and C═S modes occur at 928 cm^{-1}. The peak at 556 cm^{-1} is associated with the SS stretching mode. The peak at 486 cm^{-1} is due to the CH_3NC deformation and C═S stretching modes. The S═CS deformation and the CSS deformation occur at 339 cm^{-1}.

SERS calibration curve

Thiram is a dithiocarbamate fungicide which has a disulfide bond. It is known that there is cleavage of the disulfide bond upon exposure to gold nanoparticles or gold substrates.[46] When the disulfide bond in thiram breaks, it can bind to the dogbone shaped gold nanoparticles *via* the gold thiolate bond. Different concentrations of thiram are added to the dogbone shaped gold nanoparticles and allowed to bind overnight. The SERS spectra were obtained in triplicate sets for different concentrations of thiram that is covalently bound to the smaller dogbone shaped gold nanoparticles. Fig. 6 shows a representative raw SERS spectra as well as the calibration curve of the SERS intensity as a function of the thiram concentration obtained by using the smaller dogbone shaped gold nanoparticles. The error bars represent the standard deviation of the average Raman intensity (counts per 30 s) obtained with three sets of SERS measurement. It can be seen from the linear fit that the SERS measurements are reproducible. The limit of detection (LOD) is determined by first calculating the minimum distinguishable signal which is the average signal of the blank + 3 times the standard deviation of the blank. The minimum distinguishable signal is then plugged into the best-fit equation of the calibration curve to calculate the limit of detection. The limit of detection obtained for thiram by using the smaller dogbone shaped gold nanoparticles is 43.9 ± 6.2 nM.

Fig. 7 shows a representative set of raw SERS spectra from triplicate sets as well as the calibration curve of the SERS

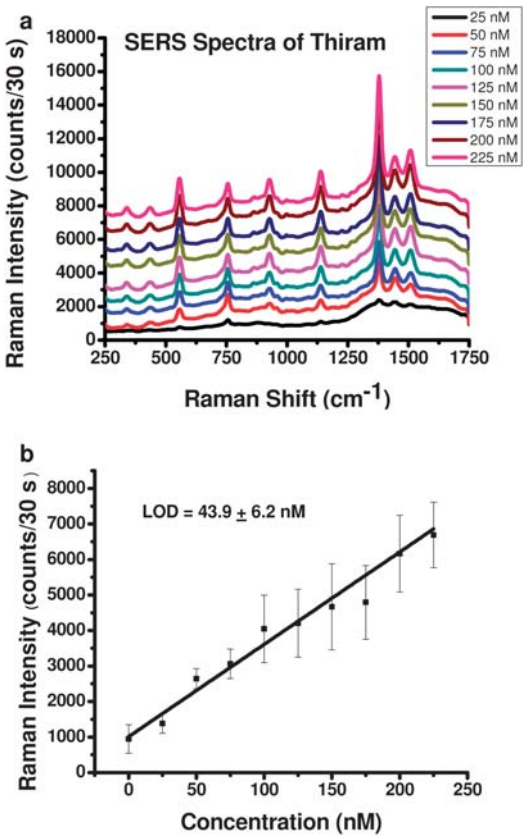

Fig. 6 Raw SERS spectra (a) and SERS calibration curve of SERS intensity with 30 second integration time as a function of the thiram concentration obtained by using the smaller dogbone shaped gold nanoparticles as colloidal SERS substrates (b).

intensity as a function of the thiram concentration obtained by using the larger dogbone shaped gold nanoparticles. The error bars represent the standard deviation of the average Raman intensity (countsper 30 s) obtained with three sets of SERS measurement. It can be seen from the linear fit that the SERS measurements are reproducible. In the case of the larger dogbone shaped Au nanoparticles, the limit of detection is 11.8 ± 3.2 nM. Using the larger dogbone shaped Au nanoparticles as colloidal SERS substrates results in 3.7× lower limit of detection. Several sources that give rise to the higher SERS enhancements are discussed in the next section.

Sources of higher SERS activities

It has been previously shown that cubic, block, and dogbone shaped gold nanoparticles result in ~100× higher SERS enhancements for 4-mercaptobenzoic acid compared to spherical nanoparticles.[39] In the case of these nanoparticles, the higher SERS enhancements are attributed to the lightning rod effect. The two types of dogbone shaped gold nanoparticles that we have synthesized have a similar concentration in which the smaller nanoparticles have a concentration of 1.25×10^{11} nanoparticles per mL and the larger dogbone shaped gold nanoparticles have a concentration of 1.13×10^{11} nanoparticles per mL. In the case of our smaller dogbone shaped gold nanoparticles, the source of the SERS enhancement is due to the

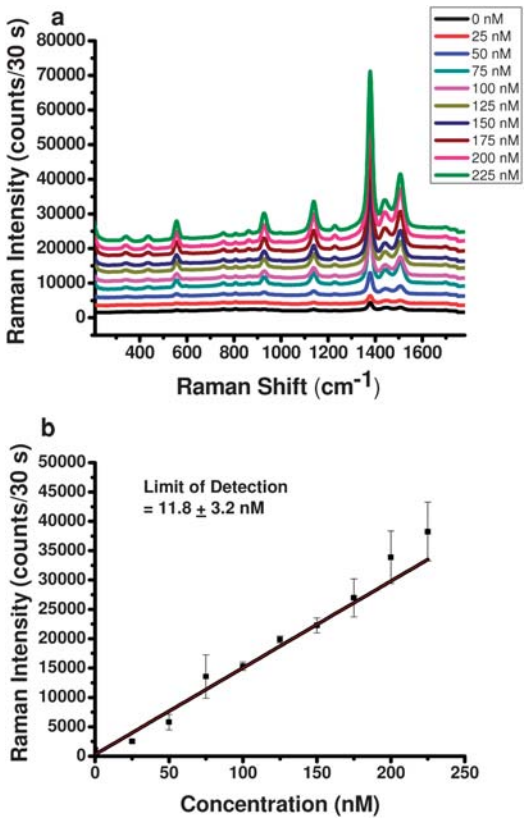

Fig. 7 Raw SERS spectra (a) and SERS calibration curve of SERS intensity with 30 second integration time as a function of the thiram concentration obtained by using the larger dogbone shaped gold nanoparticles as colloidal SERS substrates (b).

lightning rod effect in which there are greater electromagnetic fields at the corners and edges of the nanoparticles. In the case of the larger dogbone shaped gold nanoparticles, in addition to the lightning rod effect, there are much greater contributions from the electromagnetic enhancement effect since the surface plasmon band λ_{max} is 758 nm which is close to the laser excitation wavelength of 785 nm. This gives rise to some of the higher SERS enhancement that is observed. Also, since the surface area of the larger dogbone shaped gold nanoparticles (6276.07 nm^2) is larger than the surface area of the smaller dogbone shaped gold nanoparticles (5175.85 nm^2) more thiram can bind to the nanoparticle surface resulting in some of the higher enhancements that is observed. Overall, there are higher SERS enhancements and lower limits of detection for thiram observed for the larger dogbone shaped gold nanoparticles. The sources that contribute to the higher SERS enhancements and lower limits of detection observed for the larger dogbone shaped gold nanoparticles are lightning rod effect, surface plasmon band λ_{max} being in much greater resonance to the laser excitation wavelength resulting in greater contributions from the electromagnetic enhancement effect, and more surface sites for thiram to bind to the nanoparticle surface due to a higher surface area.

Conclusions

We have developed a quantitative analytical solution-based direct readout SERS method for detection of thiram which is a dithiocarbamate fungicide. Two different sizes of dogbone shaped gold nanoparticles are used as colloidal SERS substrates for SERS based detection of thiram. It is observed that using larger dogbone shaped gold nanoparticles results in lower limits of detection compared to using the smaller dogbone shaped gold nanoparticles. The lower limits of detection observed for the larger dogbone shaped gold nanoparticles could be attributed to the lightning rod effect, surface plasmon band λ_{max} being in much greater resonance to the laser excitation wavelength, and more surface sites for thiram to bind. There are higher contributions in the SERS intensities from the electromagnetic enhancement effect.

Acknowledgements

We thank Dr Richard Kingsley at the Electron Microscopy Facility for assistance in acquiring the TEM images. We thank the University of Rhode Island start-up funds, RI-INBRE Pilot Program, as well as the Society for Analytical Chemists of Pittsburgh starter grant for funding of this work.

References

1 D. L. Jeanmaire and R. P. VanDuyne, Surface Raman spectroelectrochemistry. Part I. Heterocyclic, aromatic, and aliphatic amines adsorbed on the anodized silver electrode, *J. Electroanal. Chem.*, 1977, **84**, 1.
2 M. G. Albrecht and J. A. Creighton, Anomalously intense Raman spectra of pyridine at a silver electrode, *J. Am. Chem. Soc.*, 1977, **99**, 5215.
3 M. Moskovits, Surface-enhanced Raman spectroscopy. A brief perspective, *Top. Appl. Phys.*, 2006, **103**, 1.
4 J. A. Dieringer, A. D. McFarland, N. C. Shah, D. A. Stuart, A. V. Whitney, C. R. Yonzon, M. A. Young, X. Zhang and R. P. Van Duyne, Surface enhanced Raman spectroscopy: new materials, concepts, characterization tools, and applications, *Faraday Discuss.*, 2006, **132**, 9.
5 C. L. Haynes, A. D. McFarland and R. P. VanDuyne, Surface-enhanced Raman spectroscopy, *Anal. Chem.*, 2005, **77**(17), 338A–346A.
6 M. Moskovits, Surface-enhanced Raman spectroscopy: a brief retrospective, *J. Raman Spectrosc.*, 2005, **36**(6–7), 485.
7 W. E. Smith, K. Faulds and D. Graham, Quantitative surface-enhanced resonance Raman spectroscopy for analysis, *Top. Appl. Phys.*, 2006, **103**, 381.
8 C. L. Haynes, C. R. Yonzon, X. Zhang and R. P. VanDuyne, Surface-enhanced Raman sensors: early history and the development of sensors for quantitative biowarefare agent and glucose detection, *J. Raman Spectrosc.*, 2005, **36**(6–7), 471.
9 S. C. Pinzaru, I. Pavel, N. Leopold and W. Kiefer, Identification and characterization of pharmaceuticals using Raman and surface-enhanced Raman scattering, *J. Raman Spectrosc.*, 2004, **35**(5), 338.
10 T. Vo-Dinh, SERS chemical sensors and biosensors: new tools for environmental and biological analysis, *Sens. Actuators, B*, 1995, **B29**(1–3), 183.
11 K. Faulds, W. E. Smith and D. Graham, DNA detection by surface enhanced resonance Raman scattering (SERRS), *Analyst*, 2005, **130**(8), 1125–1131.
12 A. E. Grow, L. L. Wood, J. L. Claycomb and P. A. Thompson, New biochip technology for label-free detection of pathogens and their toxins, *J. Microbiol. Methods*, 2003, **53**(2), 221–233.
13 K. Kneipp, H. Kneipp, I. Itzkan, R. R. Dasari and M. S. Feld, Surface-enhanced Raman scattering and biophysics, *J. Phys.: Condens. Matter*, 2002, **14**(18), R597–R624.
14 A. G. Ryder, Surface enhanced Raman scattering for narcotic detection and applications to chemical biology, *Curr. Opin. Chem. Biol.*, 2005, **9**(5), 489–493.
15 Z. Q. Tian, Surface-enhanced Raman spectroscopy: advancements and applications, *J. Raman Spectrosc.*, 2005, **36**(6–7), 466–470.

16 T. Vo-Dinh, Surface-enhanced Raman spectroscopy using metallic nanostructures, *TrAC, Trends Anal. Chem.*, 1998, **17**(8–9), 557–582.
17 T. Vo-Dinh, D. L. Stokes, in *Surface-Enhanced Raman scattering (SERS) for Biomedical Diagnostics*, 2003, pp 64/1–64/39.
18 T. Vo-Dinh, F. Yan and D. L. Stokes, Plasmonics-based nanostructures for surface-enhanced Raman scattering bioanalysis, *Methods Mol. Biol.*, 2005, **300**, 255–283, Protein Nanotechnology.
19 S. Xu, X. Ji, W. Xu, B. Zhao, X. Dou, Y. Bai and Y. Ozaki, Surface-enhanced Raman scattering studies on immunoassay, *J. Biomed. Opt.*, 2005, **10**(3), 031112.
20 W. E. Doering, M. E. Piotti, M. J. Natan and R. G. Freeman, *Adv. Mater.*, 2007, **19**(20), 3100.
21 R. G. Freeman, W. E. Doering, I. D. Walton, S. G. Penn, G. Davis, F. Wong and M. J. Natan, *Proc. SPIE*, 2005, **5705**, 114.
22 S. P. Mulvaney, M. D. Musick, C. D. Keating and M. J. Natan, *Langmuir*, 2003, **19**(11), 4784.
23 M. El-Kouedi, C. D. Keating, *Nanobiotechnology*, 2004, p. 429.
24 G. A. Baker and D. S. Moore, Progress in plasmonic engineering of surface-enhanced Raman-scattering substrates toward ultra-trace analysis, *Anal. Bioanal. Chem.*, 2005, **382**(8), 1751–1770.
25 K. M. Spencer, J. M. Sylvia, P. J. Marren, J. F. Bertone and S. D. Christesen, Surface-enhanced Raman spectroscopy for homeland defense, *Proc. SPIE*, 2004, **5269**, 1–8, Chemical and Biological Point Sensors for Homeland Defense.
26 W. E. Smith, P. C. White, C. Rodger and G. Dent, Raman and surface enhanced resonance Raman scattering: applications in forensic science, *Pract. Spectrosc.*, 2001, **28**, 733–748, Handbook of Raman Spectroscopy.
27 A. M. Alak and D. Tuan Vo, Surface-enhanced Raman spectrometry of chlorinated pesticides, *Anal. Chim. Acta*, 1988, **206**(1–2), 333–337.
28 S. Bonora, M. Di Foggia and M. Iafisco, SERS in the analysis of pesticides (triazinic herbicides), *Chim. Ind.*, 2008, **90**(10), 98–100.
29 C. J. Lee, H. J. Kim, M. R. Karim and M. S. Lee, Surface-enhanced Raman spectroscopy of ethephone adsorbed on silver surface, *Bull. Korean Chem. Soc.*, 2006, **27**(4), 545–548.
30 D. Lee, S. Lee, G. H. Seong, J. Choo, E. K. Lee, D.-G. Gweon and S. Lee, Quantitative analysis of methyl parathion pesticide in a polydimethylsiloxane microfluidic channel using confocal surface-enhanced Raman spectroscopy, *Appl. Spectrosc.*, 2006, **60**(4), 373–377.
31 V. Lee and S. Farquharson, SERS sample vials based on sol–gel process for trace pesticide analysis, *Proc. SPIE*, 2001, **4206**, 140–146, Photonic Detection and Intervention Technologies for Safe Food.
32 J. Qiao, G. Zheng and F. Li, Determination of trace pesticide in water by surface enhanced Raman spectroscopy, *Huaxue Tongbao*, 2006, **69**(6), 462–464.
33 C. Shende, A. Gift, F. Inscore, P. Maksymiuk and S. Farquharson, Inspection of pesticide residues on food by surface-enhanced raman spectroscopy, *Proc. SPIE*, 2004, **5271**, 28–34, Monitoring Food Safety, Agriculture, and Plant Health.
34 C. S. Shende, F. Inscore, A. Gift, P. Maksymiuk and S. Farquharson, Analysis of pesticides on or in fruit by surface-enhanced Raman spectroscopy, *Proc. SPIE*, 2004, **5587**, 170–176, Nondestructive sensing for food Safety, Quality, and Natural Resources.
35 J. S. Kang, S. Y. Hwang, C. J. Lee and M. S. Lee, SERS of dithiocarbamate pesticides adsorbed on silver surface; thiram, *Bull. Korean Chem. Soc.*, 2002, **23**(11), 1604–1610.
36 M. S. Kim, J. S. Kang, S. B. Park and M. S. Lee, Surface-enhanced Raman spectroscopy of quinomethionate adsorbed on silver colloids, *Bull. Korean Chem. Soc.*, 2003, **24**(5), 633–637.
37 S. Sanchez-Cortes, C. Domingo, J. V. Garcia-Ramos and J. A. Aznarez, Surface-enhanced vibrational study (SEIR and SERS) of dithiocarbamate pesticides on gold films, *Langmuir*, 2001, **17**(4), 1157–1162.
38 S. Sanchez-Cortes, M. Vasina, O. Francioso and J. V. Garcia-Ramos, Raman and surface-enhanced Raman spectroscopy of dithiocarbamate fungicides, *Vib. Spectrosc.*, 1998, **17**(2), 133–144.
39 C. J. Orendorff, A. Gole, T. K. Sau and C. J. Murphy, Surface-enhanced Raman spectroscopy of self-assembled monolayers: sandwich architecture and nanoparticle shape dependence, *Anal. Chem.*, 2005, **77**(10), 3261–3266.
40 L. Gou and C. J. Murphy, Fine-tuning the shape of gold nanorods, *Chem. Mater.*, 2005, **17**(14), 3668–3672.
41 C. J. Murphy, T. K. Sau, A. M. Gole, C. J. Orendorff, J. Gao, L. Gou, S. E. Hunyadi and T. Li, Anisotropic metal nanoparticles: synthesis, assembly, and optical applications, *J. Phys. Chem. B*, 2005, **109**(29), 13857–13870.
42 T. K. Sau and C. J. Murphy, Room temperature, high-yield synthesis of multiple shapes of gold nanoparticles in aqueous solution, *J. Am. Chem. Soc.*, 2004, **126**(28), 8648–8649.
43 A. Torreggiani, Z. Jurasekova, M. D'Angelantonio, M. Tamba, J. V. Garcia-Ramos and S. Sanchez-Cortes, Fabrication of Ag nanoparticles by 1-irradiation: application to surface-enhanced Raman spectroscopy of fungicides, *Colloids Surf., A*, 2009, **339**, 60–67.
44 S. Sanchez-Cortes, M. Vasina, O. Francioso and J. V. Garcia-Ramos, Raman and surface-enhanced Raman spectroscopy of dithiocarbamate fungicides, *Vib. Spectrosc.*, 1998, **17**, 133–144.
45 S. Sanchez-Cortes, C. Domingo, J. V. Garcia-Ramos and J. A. Aznarez, Surface-enhanced vibrational study (SEIR and SERS) of dithiocarbamate pesticides on gold films, *Langmuir*, 2001, **17**, 1157–1162.
46 H. A. Biebuyck and G. M. Whitesides, Interchange between monolayers on gold formed from unsymmetrical disulfides and solutions of thiols: evidence for sulfur-sulfur bond cleavage by gold metal, *Langmuir*, 1993, **9**(7), 1766–1770.